

ARFA: An Asymmetric Receptive Field Autoencoder Model for Spatiotemporal Prediction

Wenxuan Zhang^{1,*}, Xuechao Zou^{1,*}, Li Wu^{1,†}, Jianqiang Huang¹, Xiaoying Wang¹
¹Department of Computer Technology and Applications, Qinghai University, Xining, China
{iezhangwenxuan, xuechaozou, wuli_qhu, hjqxaly, Wangxiaofu163}@163.com

Abstract

Spatiotemporal prediction aims to generate future sequences by paradigms learned from historical contexts. It holds significant importance in numerous domains, including traffic flow prediction and weather forecasting. However, existing methods face challenges in handling spatiotemporal correlations, as they commonly adopt encoder and decoder architectures with identical receptive fields, which adversely affects prediction accuracy. This paper proposes an Asymmetric Receptive Field Autoencoder (ARFA) model to address this issue. Specifically, we design corresponding sizes of receptive field modules tailored to the distinct functionalities of the encoder and decoder. In the encoder, we introduce a large kernel module for global spatiotemporal feature extraction. In the decoder, we develop a small kernel module for local spatiotemporal information reconstruction. To address the scarcity of meteorological prediction data, we constructed the RainBench, a large-scale radar echo dataset specific to the unique precipitation characteristics of inland regions in China for precipitation prediction. Experimental results demonstrate that ARFA achieves consistent state-of-the-art performance on two mainstream spatiotemporal prediction datasets and our RainBench dataset, affirming the effectiveness of our approach. This work not only explores a novel method from the perspective of receptive fields but also provides data support for precipitation prediction, thereby advancing future research in spatiotemporal prediction.

1. Introduction

Spatiotemporal prediction [1] is an important and challenging task that involves the comprehensive analysis of spatial and temporal data. With the advent of the big data era, we are faced with massive amounts of spatiotemporal data containing rich information that can provide valuable

clues for future predictions. Spatiotemporal prediction not only focuses on temporal trends and changes but also considers spatial correlations. Its applications are widespread, ranging from precipitation forecasting [2, 3, 4] to urban traffic planning [5, 6], from environmental monitoring [7] to social media analysis [8], all of which rely on the prediction and analysis of spatiotemporal data.

Currently, numerous methods have been proposed to address the challenges in spatiotemporal prediction. These methods include statistical time series models, traditional machine learning algorithms [8], deep learning models [9, 10, 11, 12], and simulation approaches based on physical models [13]. Among them, deep learning methods have made significant advancements in the field of spatiotemporal prediction, particularly with the introduction of Convolutional Neural Networks (CNNs) [14, 15, 16, 17] and Recurrent Neural Networks (RNNs) [18, 19], enabling more accurate and efficient modeling and prediction of spatiotemporal data. Currently, mainstream deep learning models applied in spatiotemporal prediction can be broadly categorized into three types: pure CNN models [20, 21], pure RNN models [22, 23], and hybrid models combining CNNs and RNNs. CNN models were initially designed to address problems such as image recognition and have been subsequently applied to spatial feature extraction in temporal data. The operation of CNNs can be understood as the process of extracting similar features at multiple positions in an image using a small number of parameters. RNN, short for Recurrent Neural Network, is a type of neural network specifically designed to handle variable-length data. Long Short-Term Memory (LSTM [22]) and Gated Recurrent Unit (GRU [24]) are the most commonly used units for spatiotemporal prediction. They include feedback connections that provide the network with a form of memory for previous signals, allowing it to learn from experience, and thus are well-suited for modeling long-term correlations in spatiotemporal prediction.

However, spatiotemporal prediction still faces several challenges. Previous models, including both encoder and decoder components, have utilized modules with the same

*These authors contributed equally.

†Corresponding author.

receptive field size without specific optimization. We observe that different receptive field sizes are required in the encoding and decoding stages of the model. Therefore, a symmetric autoencoder structure restricts the transfer of spatiotemporal information between the encoder and decoder, making it difficult for the model to capture complex feature patterns in the temporal data. Additionally, meteorological prediction is one of the most prevalent applications in spatiotemporal prediction, yet there is currently a lack of relevant data to support this research.

To address these challenges, this paper proposes a novel Asymmetric Receptive Field Autoencoder (ARFA) model. We address the different functionalities of the encoder and decoder by designing processing modules with corresponding receptive field sizes. The encoder module is designed for global spatiotemporal feature extraction, and thus, we introduce a large kernel module to provide an approximate global receptive field. The decoder module is responsible for spatiotemporal information reconstruction, and to achieve this, we develop a small kernel module to recover local fine structures. Additionally, to tackle the issue of missing meteorological prediction data, we construct a large-scale precipitation prediction dataset called RainBench, which contains 63,200 spatiotemporal sequences. Each sequence consists of ten input frames and ten target frames, with each frame’s image size being 200×200 .

In summary, the contributions of our work can be summarized as follows:

- We propose a novel Asymmetric Receptive Field Autoencoder (ARFA) model that combines global encoding and local decoding to achieve high-precision spatiotemporal prediction.
- We design two novel modules for the encoder and decoder: the Large Kernel Module and the Small Kernel Module, leveraging the advantages of different-sized convolutional kernels for global spatiotemporal feature extraction and local fine structure reconstruction.
- We create a large-scale radar echo dataset for precipitation prediction, named RainBench, with the potential to serve as a benchmark for future spatiotemporal forecasting endeavors.

Building upon the aforementioned contributions, we have developed a highly accurate spatiotemporal prediction model. In comparison to existing approaches, our proposed ARFA consistently achieves state-of-the-art performance on two prominent spatiotemporal prediction datasets, namely Moving-MNIST [25] and KTH [26], as well as on our custom RainBench dataset. These results serve as compelling evidence of the effectiveness of ARFA. To facilitate further research in this direction, we intend to

release the source code, pre-trained models, and datasets associated with our work.

2. Related Work

2.1. Spatiotemporal Prediction

Spatiotemporal prediction involves forecasting the values, states, or events in the future given a sequence of spatiotemporal observational data. It holds significant research significance and practical value across various domains and applications. However, the prediction process in the spatiotemporal domain is highly complex due to the spatial and temporal variations in the joint distribution of neighboring pixel values. Consequently, deep learning networks based on Convolutional Neural Networks (CNNs) and Recurrent Neural Networks (RNNs) have been widely employed to capture spatial correlations and temporal dependencies in spatiotemporal sequences.

Ranzato et al. [27] constructed an RNN model for predicting the next frame. Srivastava et al. [28] employed LSTM for multi-frame prediction. Shi et al. [29] extended LSTM by introducing convolutional operations within the recurrent connections, proposing ConvLSTM to better capture spatiotemporal correlations. They utilized ConvLSTM to establish an end-to-end trainable model for short-term precipitation forecasting. Finn et al. [30] developed an action-conditioned prediction model explicitly predicting pixel motion distribution from the previous frame. PredRNN [10] addressed the issue of gradient vanishing and exploding, which hindered the traditional RNN models in capturing long-term memory information, by introducing gating mechanisms and recursive prediction strategies based on ConvLSTM. Wang et al. [11] improved PredRNN by introducing a Gradient Highway Unit with a multi-level structure and random weight masking. E3D-LSTM [31] integrated 3D convolutions into RNN, enabling the encapsulated 3D-Conv to serve as a motion perception module and allowing memory cells to store better short-term features. MIM [32] employed a self-updating memory module to simulate the non-stationary and stationary features of videos. PhyDnet [19] introduced a dual-branch deep architecture and proposed a novel recurrent physical cell (PhyCell) to address the challenges of handling missing data and long-term prediction. MAU [18] captured reliable inter-frame motion information by widening the temporal receptive field of prediction units. With lower computational load, MAU can be easily applied to other prediction models. PredRNNv2 [33] introduced a decoupling loss in the basic structural unit of the original PredRNN, enabling the upper and lower parts of the ST-LSTM structure to better focus on different aspects of spatiotemporal changes. However, the aforementioned methods have not considered the design of the autoencoder decoder from the perspective of recep-

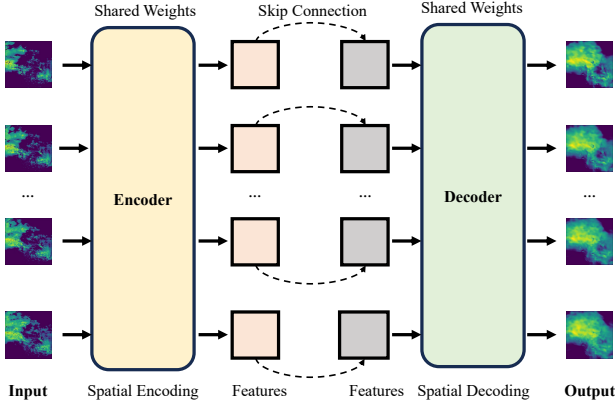


Figure 1. Overall pipeline for spatiotemporal prediction using the encoder and decoder with shared weights.

tive fields. In this regard, we propose a novel autoencoder model with asymmetric receptive fields to achieve higher spatiotemporal prediction performance.

2.2. Large Kernel Networks

Large kernel convolutions [34, 35, 36] are commonly used operations in CNNs to handle input feature maps with larger scales. By increasing the size of the convolutional kernel, large kernel convolutions can expand the receptive field and capture a broader context of information. Swin Transformer [37, 38, 39, 40] and PVT [41] have gained wide application in computer vision due to their effectiveness in image recognition tasks. [37, 38, 39, 40] has demonstrated that large receptive fields are a key factor in their success. In light of this, recent studies have shown that well-designed convolutional networks with large receptive fields can be highly competitive with transformer-based models. For instance, ConvNeXt [34] employs 7×7 depthwise separable convolutions in its backbone, significantly improving the performance of downstream tasks.

Additionally, RepLKNet [36] achieves remarkable performance by reparameterizing with 31×31 convolutional kernels. SLaK [42] further extends the kernel size to 51×51 using kernel decomposition and sparse group techniques. VAN [43] introduces an efficient large kernel decomposition as convolutional attention. Similarly, SegNeXt [44] and Conv2Froft [45] demonstrate the importance of large kernel convolutions in capturing richer context-modulated convolutional features. While large kernel convolutions have received attention in general object recognition tasks, research in the field of spatiotemporal sequence prediction is lacking. It is easily observed that spatiotemporal sequence data contains abundant contextual information, making large kernel convolutions particularly suitable for feature encoding in spatiotemporal prediction tasks.

3. Method

3.1. Overall Pipeline

Spatiotemporal prediction aims to generate output frames of images from a set of temporally correlated input image frames, as illustrated in Figure 1. Here, we define the set of input frames as $\mathbf{x} \in \mathbb{R}^{M \times C \times H \times W}$, and the output image frames as $\hat{\mathbf{y}} \in \mathbb{R}^{N \times C \times H \times W}$. M and N denote the lengths of the input and output temporal sequences, respectively, while C , H , and W represent the number of channels, height, and width of a single image frame. We assume that for any given input image frame \mathbf{x} , there exists a deterministic temporal correlation between its preceding and succeeding frames, implying a regular variation in pixel values over time.

The objective of spatiotemporal prediction is to learn patterns of spatiotemporal evolution from input frames and subsequently simulate future trends. Initially, the spatiotemporal sequence \mathbf{x} is fed into an encoder, which encodes the spatial information and temporal relationships of \mathbf{x} into abstract features. Each temporal step’s feature becomes an intermediate representation of the transitional state. Subsequently, spatial decoding is performed using a decoder. To further enhance the modeling of contextual information and the model’s multi-scale perception capability, skip connections are explicitly introduced within the same feature scale hierarchy. Additionally, for efficiency considerations, both the encoder and decoder employ weight sharing, aiming to reduce parameter complexity and computational overhead.

3.2. Asymmetric Receptive Field Autoencoder

We propose an autoencoder model with an asymmetric receptive field architecture to enhance spatiotemporal prediction accuracy. As illustrated in Figure 2, our model, named ARFA, employs distinct scales of receptive field modules in the encoder and decoder. We observe that this asymmetric receptive field design maximally accommodates the diverse functionalities of the encoder and decoder, leading to improved performance.

3.2.1 Encoder with Large Receptive Field

The objective of an encoder is to transform an input sequence into a high-dimensional feature representation. However, traditional encoder architectures [46, 47, 48] may have limitations in capturing long-range dependency relationships due to their limited receptive field. This limitation becomes more significant as the temporal span for predicting frames increases. Motivated by this consideration, we propose a novel residual structure called the Large Kernel Module (LKM) for the encoder, enabling it to capture

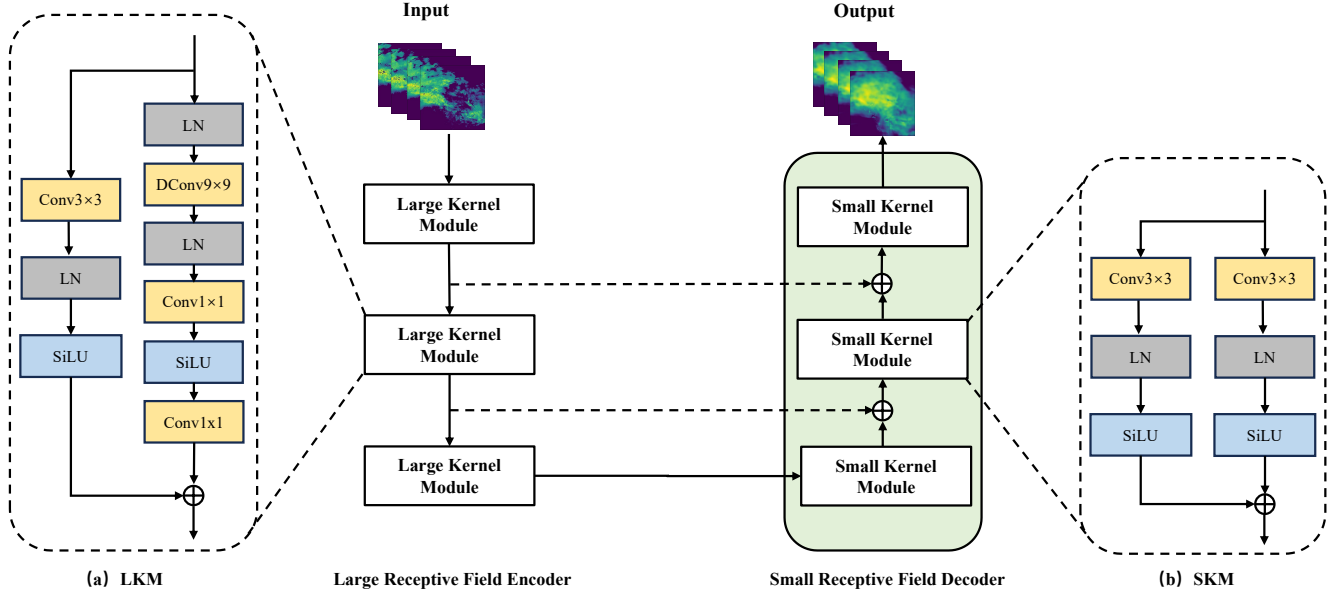


Figure 2. Overall architecture of our proposed ARFA. ARFA is an autoencoder consisting of carefully designed Large Kernel Modules (LKM) and Small Kernel Modules (SKM), serving as the encoder and decoder, respectively. The LKMs offer a large receptive field for global feature extraction in the encoder, while the decoder utilizes SKMs for local information reconstruction.

longer-distance dependencies and extract more comprehensive global contextual information.

Specifically, the LKM consists of two parallel branches: the main branch and the residual branch. The main branch primarily comprises a large kernel convolution and a Multi-Layer Perceptron (MLP). The large kernel convolution employs a 9×9 depth-wise separable convolution, which incurs a small increase in parameter count to achieve a larger receptive field. Subsequently, to compensate for the performance degradation caused by the lack of channel interactions in depth-wise separable convolutions [49], we introduce an MLP composed of two 1×1 convolutions and a SiLU [50] to recalibrate the features. Ultimately, the main branch outputs a global feature.

$$\mathbf{F}_{global} = \text{MLP}(\text{DConv}_{9 \times 9}(\mathbf{F}_{in})), \quad (1)$$

where $\mathbf{F}_{in} \in \mathbb{R}^{M \times C \times H \times W}$ denotes the input features, DConv refers to depthwise separable convolution, and \mathbf{F}_{global} represents the features outputted by the main branch of LKM. For the sake of brevity, certain details such as reshaping and normalization have been omitted.

The residual branch, on the other hand, primarily consists of a convolutional layer with a 3×3 kernel size, which facilitates the extraction of local features. Moreover, layer normalization is introduced to stabilize the training process.

$$\mathbf{F}_{local} = \sigma(\phi(\text{Conv}_{3 \times 3}(\mathbf{F}_{in}))), \quad (2)$$

where σ denotes the activation function, ϕ refers to layer

normalization, and Conv presents standard convolution.

3.2.2 Decoder with Small Receptive Field

The decoder plays a pivotal role in the generation of high-quality outputs. It is worth noting that the functions of decoders and encoders are distinct; a decoder does not necessitate as large a receptive field as an encoder. A smaller receptive field is advantageous in capturing the local information of the input image more effectively, enabling the decoder to pay greater attention to details and local textures, thereby enhancing the quality of image reconstruction. Moreover, decoders with smaller receptive fields typically possess fewer parameters and computational requirements, thus consuming less computational resources during runtime and facilitating a more rapid generation of outputs. Motivated by these insights, we have developed a novel Small Kernel Module (SKM), designed to leverage multi-head mechanisms [51] to augment the decoder’s ability for local reconstruction.

Specifically, the SKM is a multi-headed structure consisting of two parallel convolutional branches. Each branch is composed of a 3×3 convolution, a layer normalization, and a SiLU activation function. Finally, the locally fine-grained features extracted from the two branches are fused through an additive operation to further acquire robust features. The specific formulation is given as follows:

$$\mathbf{F}_{out} = \sigma(\phi(\mathbf{F}_{global} + \mathbf{F}_{local})), \quad (3)$$

Table 1. A comparative analysis of our constructed RainBench dataset and two prominent spatiotemporal prediction datasets.

Dataset	Moving-MNIST [25]	KTH [26]	RainBench (Ours)
Train Sample	10000	5200	31600
Test Sample	10000	3167	31600
Frame Size	64×64	128×128	200×200
Input Length	10	10	10
Output Length	10	10	10

where \mathbf{F}_{out} denotes the output features.

3.3. Loss Function

The objective of the spatiotemporal prediction is to forecast future spatiotemporal states based on historical observational data. The prediction results are commonly measured using the mean squared error (MSE) metric, which quantifies the difference between the predicted values and the ground truth values. The spatiotemporal prediction network is optimized by minimizing this MSE loss function. The formulation of the loss function is given by:

$$\mathcal{L} = \|\mathbf{y} - \hat{\mathbf{y}}\|_2 = \|\mathbf{y} - f_\theta(\mathbf{x})\|_2, \quad (4)$$

where \mathbf{x} and $\hat{\mathbf{y}}$ represent the input and output sequences, respectively. \mathbf{y} denotes the ground truth values, and f_θ represents the parameterized spatiotemporal prediction model.

4. Dataset

To address the issue of data scarcity in the application of spatiotemporal prediction in the field of meteorology, we have constructed a large-scale radar echo dataset called RainBench for precipitation forecasting. A comparative analysis was conducted with the mainstream spatiotemporal prediction datasets, such as Moving-MNIST [25] and KTH [26], as shown in Table 1.

4.1. Data Collection

We have collected radar echo precipitation data from the meteorological station in Yinchuan City, Ningxia Province, for the months of April to October in 2018 and 2019. The dataset comprises observations from 31 selectable altitudes, with a temporal resolution of 6 minutes. Yinchuan City is located in the upper-middle region of the Yellow River, in the northwestern part of the Loess Plateau, with a longitude ranging from 103.91E to 108.51E and a latitude ranging from 36.18N to 40.78N. This region is characterized not only by low precipitation amounts but also by uneven spatiotemporal distribution of precipitation. The primary features of precipitation in this area include infrequent occurrence of rainfall and snowfall, as well as strong water evaporation. Consequently, spatiotemporal prediction in this region poses a significant challenge.

4.2. Data Preprocessing

We selected the first layer at an altitude of 500m as the precipitation data closely approximates ground truth. To mitigate the influence of surrounding mountains, buildings, or dust on radar signal propagation, we employed the denoising method [52] to preprocess the data. Furthermore, considering the high proportion of non-precipitation days in the entire data, we filtered out data from 84 days with relatively abundant rainfall. The original images consisted of 461×461 pixels, but to reduce memory consumption, we cropped the images into patches of size 200×200. Since the maximum value of radar echoes does not exceed 70dBZ, we normalized all the data by dividing it by 70.

4.3. Final Results

Finally, we employed a sliding window approach to ensure sufficient samples due to the insufficient number of captured precipitation days. Specifically, the original data sequence was partitioned into input and target sequences using a fixed step size window. Given that radar echo data are generated every 6 minutes, to enable the model to predict precipitation over a longer time horizon (e.g., the next hour), we set the total length of the sliding window to 20 frames, where the first ten frames were designated as input frames and the latter ten frames as ground truth. Moreover, we employed a single shift step of 2 for the sliding window, resulting in a total of 1580 sequence pairs. The training and testing sets were established with a ratio of 4:1.

5. Experiments

5.1. Implementation Details

Experimental Settings. We establish a virtual Anaconda environment with Python 3.9 and PyTorch 1.10.1. The specific computational platform employed is an NVIDIA V100 32GB GPU with CUDA 11.7. The parameter configuration is as follows: the batch size for all model training is set to 16, and all ablation experiments are conducted over 200 epochs to ensure experimental fairness. We adopt the Adam optimizer [53] with an initial learning rate of 1e-3 and employ the one cycle learning rate scheduler [54] for model training. Additionally, to stabilize the training process, we employ a parameter warm-up phase consisting of 5 epochs.

Evaluation Metrics. In all experiments conducted, we employ four widely adopted metrics to comprehensively evaluate the performance of spatiotemporal prediction pre-trained models on the test set: Mean Squared Error (MSE), Mean Absolute Error (MAE), Peak Signal-to-Noise Ratio (PSNR), and Structural Similarity Index (SSIM [55]).

Table 2. Ablation study of convolution kernel size in the LKM.

Kernel Size	MSE ↓	MAE ↓	SSIM ↑	PSNR ↑
3×3	26.605	76.354	0.940	38.361
5×5	26.102	75.495	0.941	38.383
7×7	26.004	75.278	0.941	38.385
9×9	25.975	74.783	0.942	38.398
11×11	25.999	75.265	0.942	38.366

Table 3. Ablation study of receptive field size in the autoencoder.

Encoder	Decoder	MSE ↓	MAE ↓	SSIM ↑	PSNR ↑
Small	Small	27.102	78.379	0.939	38.280
Small	Large	29.973	83.104	0.932	38.114
Large	Large	28.154	78.927	0.936	38.274
Large	Small	25.306	73.892	0.944	38.434

5.2. Ablation Studies

To validate the effectiveness of our proposed asymmetric receptive field autoencoder model, we conducted thorough ablation experiments on the most popular Moving-MNIST dataset for spatiotemporal prediction.

Convolution Kernel Size in the LKM. The size of the convolution kernel is a crucial design option in the LKM, as it determines the range of information that the model can capture when processing spatiotemporal data, directly influencing the model’s receptive field. Therefore, we conducted an ablation study on the convolution kernel size in the LKM, and the results are presented in Table 2. The experiments demonstrate that as the kernel size increases, the model exhibits more effective feature extraction capabilities with the support of a larger receptive field. The optimal performance is achieved when the kernel size is set to 9×9. Further increasing the kernel size actually leads to a performance decline. This indicates that a larger receptive field is not necessarily better; performance improvement is only achieved by effectively enlarging the receptive field within a certain range. Blindly increasing the receptive field not only fails to enhance performance but also increases the number of parameters and computational complexity.

Receptive Field Size in the Autoencoder. To investigate the impact of different receptive field sizes in the encoder and decoder of the autoencoder on spatiotemporal prediction performance, we conducted four sets of ablation experiments, and the results are presented in Table 3. The experiments reveal that, in the design of the autoencoder, the optimal combination for achieving the best performance is to employ a large receptive field in the encoder and a small receptive field in the decoder. Both scenarios where the encoder adopts a small receptive field or the decoder adopts a

Table 4. Quantitative comparison of the spatiotemporal prediction performance of our ARFA with existing methods on the Moving-MNIST dataset.

Method	MSE ↓	MAE ↓	SSIM ↑	PSNR ↑
ConvLSTM [29]	34.071	97.250	0.919	37.614
PhyDNet [19]	28.207	78.501	0.937	38.133
MAU [18]	26.842	78.049	0.940	38.197
PredRNN [10]	33.472	95.148	0.917	37.792
PredRNN++ [11]	50.374	108.13	0.904	37.978
E3DLSTM [31]	44.652	83.778	0.924	39.749
PredRNNv2 [33]	27.730	80.840	0.937	38.293
SimVPv1 [20]	32.203	89.291	0.927	37.951
SimVPv2 [21]	27.102	78.379	0.939	38.280
ARFA (Ours)	25.306	73.892	0.944	38.434

Table 5. Quantitative comparison of the spatiotemporal prediction performance of our ARFA with existing methods on the KTH dataset.

Method	MSE ↓	MAE ↓	SSIM ↑	PSNR ↑
ConvLSTM	65.164	588.333	0.855	31.215
PredRNN	60.897	515.372	0.867	32.383
SimVPv2	47.541	463.063	0.903	32.740
ARFA (Ours)	42.891	403.632	0.907	33.667

Table 6. Quantitative comparison of the spatiotemporal prediction performance of our ARFA with existing methods on our RainBench dataset.

Method	MSE ↓	MAE ↓	SSIM ↑	PSNR ↑
ConvLSTM	132.936	976.618	0.797	35.737
PredRNN	128.589	877.229	0.829	36.833
PredRNN++	119.671	956.249	0.795	35.710
MIM	119.654	874.465	0.785	34.992
SimVPv2	112.383	826.336	0.834	36.732
ARFA (Ours)	109.880	809.190	0.842	36.844

large receptive field lead to performance degradation. This observation highlights the distinct roles of the encoder and decoder, indicating that they require different receptive field sizes. These findings provide strong evidence for the effectiveness of our proposed asymmetric receptive field autoencoder model.

5.3. Comparison with the State-of-the-Arts

We conducted extensive experiments to quantitatively and qualitatively compare the performance of our proposed method, ARFA, with existing methods for spatiotemporal prediction on two popular datasets, MNIST and KTH, and on our custom-built RainBench dataset.

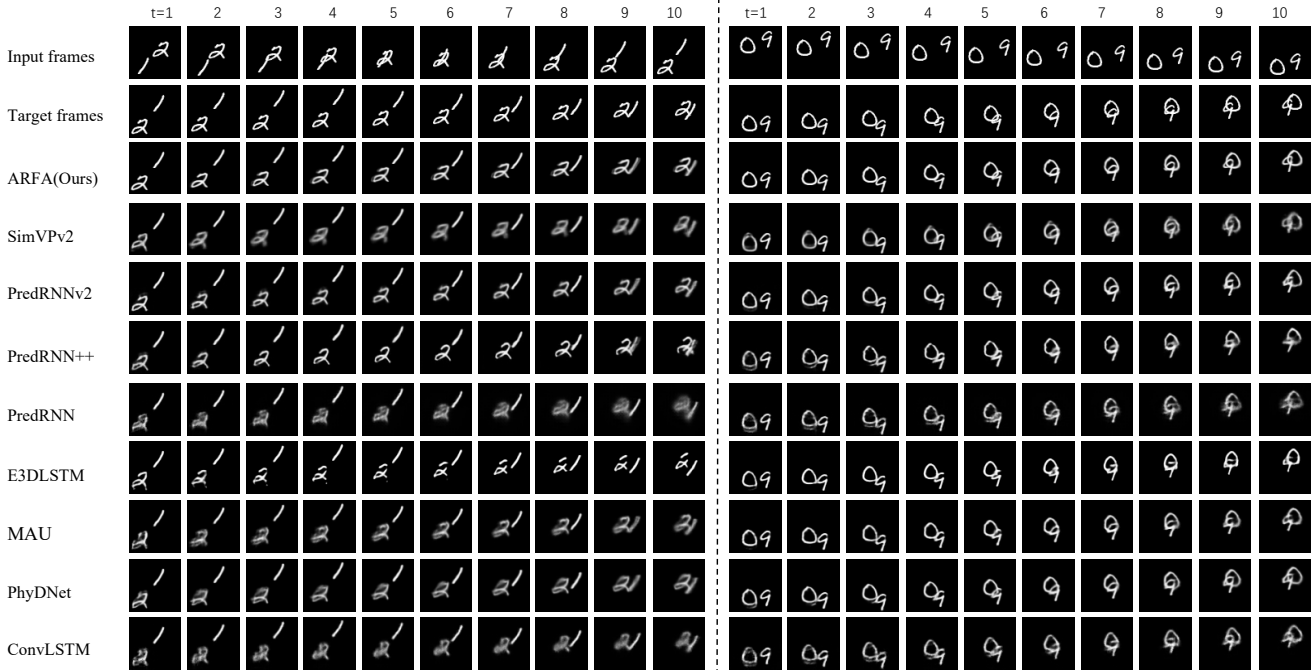


Figure 3. Visual results of our ARFA and existing methods on the Moving-MNIST dataset.

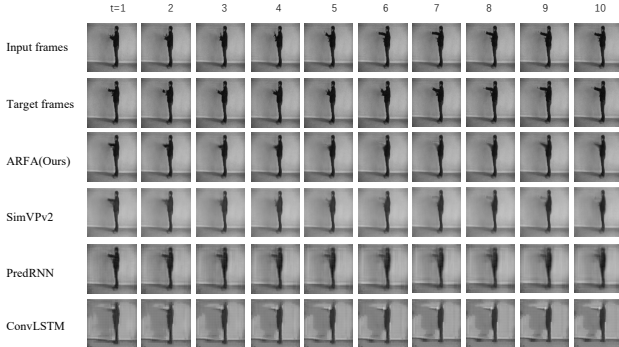


Figure 4. Visual results of our ARFA and existing methods on the KTH dataset.

Moving-MNIST. Table 4 presents the quantitative comparison results of our ARFA and existing approaches on the Moving-MNIST dataset. ARFA achieves state-of-the-art (SOTA) performance consistency across four evaluation metrics. Compared to SimVPv2, ARFA exhibits reductions of 1.796 and 4.487 in terms of MSE and MAE, respectively, while demonstrating improvements in SSIM and PSNR. As shown in Figure 3, it can be observed that ARFA consistently generates high-fidelity images, both in scenarios with non-overlapping digits (left) and overlapping digits (right). In contrast, other models, such as SimVPv2, PredRNN, and ConvLSTM, suffer from image blurring, while PredRNN++ and E3DLSTM exhibit semantic inconsistencies.

KTH. Table 5 presents the quantitative comparison results of our proposed ARFA method and existing approaches on the KTH dataset. ARFA achieves SOTA performance in terms of four evaluation metrics. Compared to SimVPv2, ARFA demonstrates a reduction of 4.650 and 59.431 in terms of MSE and MAE, respectively. Additionally, ARFA exhibits improvements in SSIM and PSNR. As depicted in Figure 4, it can be observed that SimVPv2 fails to restore the arm of the person, the generated result by PredRNN appears blurry, and ConvLSTM fails to predict the head and arms. In contrast, ARFA-generated images exhibit no such blurriness or semantic inconsistencies as mentioned above.

RainBench. Table 6 presents the quantitative comparison results of our ARFA and existing approaches on our RainBench dataset. ARFA achieves SOTA performance consistency across four evaluation metrics. Compared to SimVPv2, ARFA reduces the MSE by 2.503 and the MAE by 17.146. Moreover, ARFA exhibits improvements in both structural similarity index (SSIM) and peak signal-to-noise ratio (PSNR). As depicted in Figure 5, it can be observed that ARFA consistently outperforms other methods in terms of prediction accuracy, regardless of sparse rainfall scenarios (left) or dense rainfall scenarios (right). SimVPv2 follows as the second-best performer. However, alternative methods such as MIM, PredRNN, and ConvLSTM gradually lose the original characteristics of the generated images

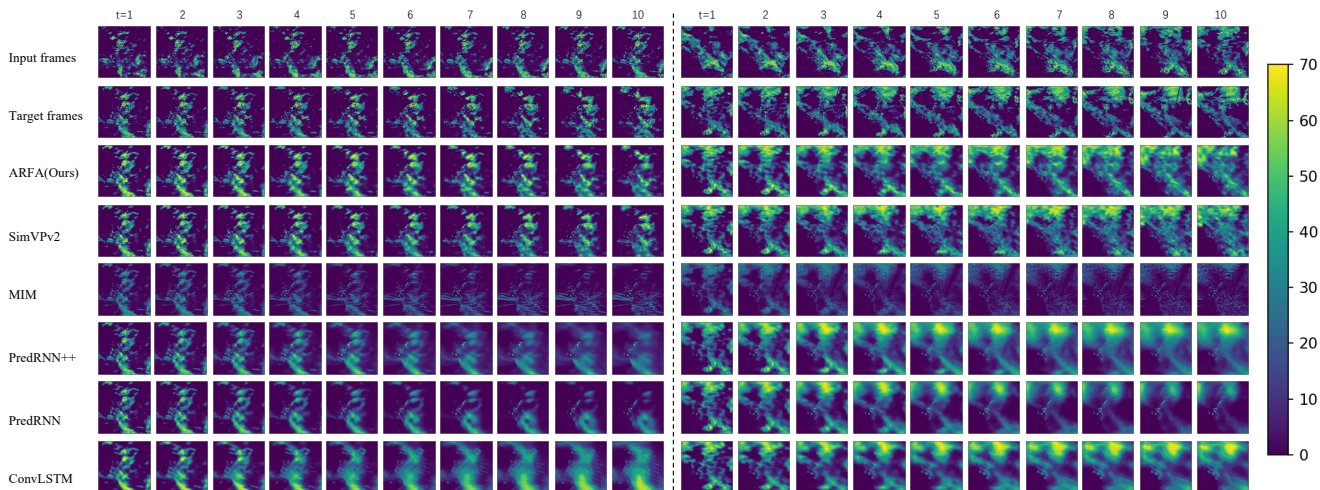


Figure 5. Visual results of our ARFA and existing methods on our RainBench dataset.

as the prediction time steps increase. Given the inherent challenges of the dataset, future research endeavors could employ RainBench as a benchmark to further explore superior spatiotemporal prediction algorithms.

6. Conclusion

This paper presented the Asymmetric Receptive Field Autoencoder (ARFA) model as a solution to the challenges of handling spatiotemporal correlations in spatiotemporal prediction. By incorporating tailored sizes of receptive field modules in the encoder and decoder architectures, the ARFA effectively improved prediction accuracy. Additionally, RainBench, a radar echo dataset specific to the precipitation characteristics of inland regions in China was collected and constructed for precipitation prediction. Experimental results confirmed the effectiveness of the proposed ARFA in improving prediction accuracy. Overall, the findings of this study contribute to the advancement of spatiotemporal prediction research, both in terms of exploring new methods and providing data resources for the meteorological domain. Future research in spatiotemporal prediction can build upon the insights and techniques presented in this paper to further enhance the accuracy and applicability of predictive models in various domains.

References

- [1] Alex Graves and Jürgen Schmidhuber. Framewise phoneme classification with bidirectional lstm and other neural network architectures. *NEURAL NETWORKS*, 18(5-6):602–610, 2005.
- [2] Michael Dixon and Gerry Wiener. Titan: Thunderstorm identification, tracking, analysis, and nowcasting—a radar-based methodology. *J ATMOS OCEAN TECH*, 10(6):785–797, 1993.
- [3] Venkatesh Kolluru, Srinivas Kolluru, Nimisha Wagle, and Tri Dev Acharya. Secondary precipitation estimate merging using machine learning: development and evaluation over krishna river basin, india. *REMOTE SENS-BASEL*, 12(18): 3013, 2020.
- [4] Kamal Ahmed, DA Sachindra, Shamsuddin Shahid, Zafar Iqbal, Nadeem Nawaz, and Najeebullah Khan. Multi-model ensemble predictions of precipitation and temperature using machine learning algorithms. *ATMOS RES*, 236:104806, 2020.
- [5] Huaxiu Yao, Xianfeng Tang, Hua Wei, Guanjie Zheng, and Zhenhui Li. Revisiting spatial-temporal similarity: A deep learning framework for traffic prediction. In *AAAI*, volume 33, pages 5668–5675, 2019.
- [6] Chuanpan Zheng, Xiaoliang Fan, Cheng Wang, and Jianzhong Qi. Gman: A graph multi-attention network for traffic prediction. In *AAAI*, volume 34, pages 1234–1241, 2020.
- [7] Federico Amato, Fabian Guignard, Sylvain Robert, and Mikhail Kanevski. A novel framework for spatio-temporal prediction of environmental data using deep learning. *SCI REP-UK*, 10(1):22243, 2020.
- [8] Peng Xie, Tianrui Li, Jia Liu, Shengdong Du, Xin Yang, and Junbo Zhang. Urban flow prediction from spatiotemporal data using machine learning: A survey. *INFORM FUSION*, 59:1–12, 2020.
- [9] Xingjian Shi, Zhihan Gao, Leonard Lausen, Hao Wang, Dit-Yan Yeung, Wai-kin Wong, and Wang-chun Woo. Deep learning for precipitation nowcasting: A benchmark and a new model. *NeurIPS*, 30, 2017.
- [10] Yunbo Wang, Mingsheng Long, Jianmin Wang, Zhifeng Gao, and Philip S Yu. Predrnn: Recurrent neural networks

- for predictive learning using spatiotemporal lstms. *NeurIPS*, 30, 2017.
- [11] Yunbo Wang, Zhifeng Gao, Mingsheng Long, Jianmin Wang, and S Yu Philip. Predrnn++: Towards a resolution of the deep-in-time dilemma in spatiotemporal predictive learning. In *International Conference on Machine Learning*, pages 5123–5132, 2018.
- [12] Haoxing Lin, Rufan Bai, Weijia Jia, Xinyu Yang, and Yongjian You. Preserving dynamic attention for long-term spatial-temporal prediction. In *KDD*, pages 36–46, 2020.
- [13] Lei Xu, Nengcheng Chen, Zeqiang Chen, Chong Zhang, and Hongchu Yu. Spatiotemporal forecasting in earth system science: Methods, uncertainties, predictability and future directions. *EARTH-SCI REV*, 222:103828, 2021.
- [14] Weibin Zhang, Yinghao Yu, Yong Qi, Feng Shu, and Yin-hai Wang. Short-term traffic flow prediction based on spatio-temporal analysis and cnn deep learning. *TRANSPORTMET-RICA A*, 15(2):1688–1711, 2019.
- [15] William Robert Johnson, Jacqueline Alderson, David Lloyd, and Ajmal Mian. Predicting athlete ground reaction forces and moments from spatio-temporal driven cnn models. *TBME*, 66(3):689–694, 2018.
- [16] Xuechao Zou, Kai Li, Junliang Xing, Yu Zhang, Shiyang Wang, Lei Jin, and Pin Tao. Diffcr: A fast conditional diffusion framework for cloud removal from optical satellite images, 2023.
- [17] Xiaolin Hu, Kai Li, Weiyi Zhang, Yi Luo, Jean-Marie Lemercier, and Timo Gerkmann. Speech separation using an asynchronous fully recurrent convolutional neural network. In *NeurIPS*, volume 34, pages 22509–22522, 2021.
- [18] Zheng Chang, Xinfeng Zhang, Shanshe Wang, Siwei Ma, Yan Ye, Xiang Xinguang, and Wen Gao. Mau: A motion-aware unit for video prediction and beyond. *NeurIPS*, 34: 26950–26962, 2021.
- [19] Vincent Le Guen and Nicolas Thome. Disentangling physical dynamics from unknown factors for unsupervised video prediction. In *CVPR*, pages 11474–11484, 2020.
- [20] Zhangyang Gao, Cheng Tan, Lirong Wu, and Stan Z Li. Simvp: Simpler yet better video prediction. In *CVPR*, pages 3170–3180, 2022.
- [21] Cheng Tan, Zhangyang Gao, Siyuan Li, and Stan Z. Li. Simvp: Towards simple yet powerful spatiotemporal predictive learning, 2023.
- [22] Sepp Hochreiter and Jürgen Schmidhuber. Long short-term memory. *NEURAL COMPUT*, 9(8):1735–1780, 1997.
- [23] Rui Fu, Zuo Zhang, and Li Li. Using lstm and gru neural network methods for traffic flow prediction. In *YAC*, pages 324–328, 2016.
- [24] Kyunghyun Cho, Bart van Merriënboer, Caglar Gulcehre, Dzmitry Bahdanau, Fethi Bougares, Holger Schwenk, and Yoshua Bengio. Learning phrase representations using rnn encoder–decoder for statistical machine translation. In *EMNLP*, page 1724, 2014.
- [25] Kiran Kumar Chandriah and Raghavendra V Naraganahalli. Rnn/lstm with modified adam optimizer in deep learning approach for automobile spare parts demand forecasting. *MULTIMED TOOLS APPL*, 80(17):26145–26159, 2021.
- [26] Lena Gorelick, Moshe Blank, Eli Shechtman, Michal Irani, and Ronen Basri. Actions as space-time shapes. *T-PAMI*, 29(12):2247–2253, 2007.
- [27] MarcAurelio Ranzato, Arthur Szlam, Joan Bruna, Michael Mathieu, Ronan Collobert, and Sumit Chopra. Video (language) modeling: a baseline for generative models of natural videos, 2016.
- [28] Nitish Srivastava, Elman Mansimov, and Ruslan Salakhudinov. Unsupervised learning of video representations using lstms. In *ICML*, pages 843–852, 2015.
- [29] Xingjian Shi, Zhoung Chen, Hao Wang, Dit-Yan Yeung, Wai-Kin Wong, and Wang-chun Woo. Convolutional lstm network: A machine learning approach for precipitation nowcasting. *NeurIPS*, 28, 2015.
- [30] Chelsea Finn, Ian Goodfellow, and Sergey Levine. Unsupervised learning for physical interaction through video prediction. *NeurIPS*, 29, 2016.
- [31] Yunbo Wang, Lu Jiang, Ming-Hsuan Yang, Li-Jia Li, Mingsheng Long, and Li Fei-Fei. Eidetic 3d lstm: A model for video prediction and beyond. In *ICLR*, 2018.
- [32] Yunbo Wang, Jianjin Zhang, Hongyu Zhu, Mingsheng Long, Jianmin Wang, and Philip S Yu. Memory in memory: A predictive neural network for learning higher-order non-stationarity from spatiotemporal dynamics. In *CVPR*, pages 9154–9162, 2019.
- [33] Yunbo Wang, Haixu Wu, Jianjin Zhang, Zhifeng Gao, Jianmin Wang, S Yu Philip, and Mingsheng Long. Predrnn: A recurrent neural network for spatiotemporal predictive learning. *T-PAMI*, 45(2):2208–2225, 2022.
- [34] Zhuang Liu, Hanzi Mao, Chao-Yuan Wu, Christoph Feichtenhofer, Trevor Darrell, and Saining Xie. A convnet for the 2020s. In *CVPR*, pages 11976–11986, 2022.
- [35] Chao Peng, Xiangyu Zhang, Gang Yu, Guiming Luo, and Jian Sun. Large kernel matters—improve semantic segmentation by global convolutional network. In *CVPR*, pages 4353–4361, 2017.
- [36] Xiaohan Ding, Xiangyu Zhang, Jungong Han, and Guiguang Ding. Scaling up your kernels to 31x31: Revisiting large kernel design in cnns. In *CVPR*, pages 11963–11975, 2022.

- [37] Ze Liu, Yutong Lin, Yue Cao, Han Hu, Yixuan Wei, Zheng Zhang, Stephen Lin, and Baining Guo. Swin transformer: Hierarchical vision transformer using shifted windows. In *ICCV*, pages 10012–10022, 2021.
- [38] Jingyun Liang, Jiezhong Cao, Guolei Sun, Kai Zhang, Luc Van Gool, and Radu Timofte. Swinir: Image restoration using swin transformer. In *ICCV*, pages 1833–1844, 2021.
- [39] Ze Liu, Jia Ning, Yue Cao, Yixuan Wei, Zheng Zhang, Stephen Lin, and Han Hu. Video swin transformer. In *CVPR*, pages 3202–3211, 2022.
- [40] Ze Liu, Han Hu, Yutong Lin, Zhuliang Yao, Zhenda Xie, Yixuan Wei, Jia Ning, Yue Cao, Zheng Zhang, Li Dong, et al. Swin transformer v2: Scaling up capacity and resolution. In *CVPR*, pages 12009–12019, 2022.
- [41] Mathias Basner and David F Dinges. Maximizing sensitivity of the psychomotor vigilance test (pvt) to sleep loss. *SLEEP*, 34(5):581–591, 2011.
- [42] Shiwei Liu, Tianlong Chen, Xiaohan Chen, Xuxi Chen, Qiao Xiao, Boqian Wu, Tommi Kärkkäinen, Mykola Pechenizkiy, Decebal Constantin Mocanu, and Zhangyang Wang. More convnets in the 2020s: Scaling up kernels beyond 51x51 using sparsity. In *ICLR*, 2023.
- [43] Meng-Hao Guo, Cheng-Ze Lu, Zheng-Ning Liu, Ming-Ming Cheng, and Shi-Min Hu. Visual attention network. *COMPUTATIONAL VISUAL MEDIA*, pages 1–20, 2023.
- [44] Meng-Hao Guo, Cheng-Ze Lu, Qibin Hou, Zhengning Liu, Ming-Ming Cheng, and Shi-Min Hu. Segnext: Rethinking convolutional attention design for semantic segmentation. *NeurIPS*, 35:1140–1156, 2022.
- [45] Qibin Hou, Cheng-Ze Lu, Ming-Ming Cheng, and Jiashi Feng. Conv2former: A simple transformer-style convnet for visual recognition, 2022.
- [46] Olaf Ronneberger, Philipp Fischer, and Thomas Brox. U-net: Convolutional networks for biomedical image segmentation. In *MICCAI*, pages 234–241, 2015.
- [47] Xuechao Zou, Kai Li, Junliang Xing, Pin Tao, and Yachao Cui. Pmaa: A progressive multi-scale attention autoencoder model for high-performance cloud removal from multi-temporal satellite imagery. 2023.
- [48] Kai Li, Runxuan Yang, and Xiaolin Hu. An efficient encoder-decoder architecture with top-down attention for speech separation. In *ICLR*, 2023.
- [49] Andrew G. Howard, Menglong Zhu, Bo Chen, Dmitry Kalenichenko, Weijun Wang, Tobias Weyand, Marco Andreetto, and Hartwig Adam. Mobilenets: Efficient convolutional neural networks for mobile vision applications, 2017.
- [50] Stefan Elfving, Eiji Uchibe, and Kenji Doya. Sigmoid-weighted linear units for neural network function approximation in reinforcement learning. *NEURAL NETWORKS*, 107:3–11, 2018.
- [51] Ashish Vaswani, Noam Shazeer, Niki Parmar, Jakob Uszkoreit, Llion Jones, Aidan N Gomez, Łukasz Kaiser, and Illia Polosukhin. Attention is all you need. *NeurIPS*, 30, 2017.
- [52] Roy De Maesschalck, Delphine Jouan-Rimbaud, and Désiré L Massart. The mahalanobis distance. *CHEMOMETR INTELL LAB*, 50(1):1–18, 2000.
- [53] Diederik P. Kingma and Jimmy Ba. Adam: A method for stochastic optimization. In *ICLR*, 2015.
- [54] Tom Schaul, Sixin Zhang, and Yann LeCun. No more pesky learning rates. In *ICML*, pages 343–351, 2013.
- [55] Alain Hore and Djemel Ziou. Image quality metrics: Psnr vs. ssim. In *ICPR*, pages 2366–2369, 2010.